JOURNAL OF GEOPHYSICAL RESEARCH, VOL. 114, A12204, doi:10.1029/2009JA014381, 2009

Statistical study of substorm timing sequence

Naiguo Lin,[1] H. U. Frey,[1] S. B. Mende,[1] F. S. Mozer,[1] R. L. Lysak,[2] Y. Song,[2] and V. Angelopoulos[3]

Received 22 April 2009; revised 14 August 2009; accepted 21 August 2009; published 4 December 2009.

[1] Observations of timing sequences of substorms expected in various onset mechanisms are examined by using a space-time diagram, which correlates observed space signatures and auroral signatures on the ground during substorm onset. Results from a statistical study of 11 substorms show that signatures in the midtail ($x \sim 15-25\ R_E$) typically occur before the ground signatures and those in the near-Earth tail ($x \sim 10\ R_E$) and that signatures in the midtail region observed prior to the substorm onset often occur at a time which was shorter than that expected from MHD wave propagation between the different regions. This suggests that the disturbance onsets in different active regions do not seem to have a simple causal relationship between them as described by the reconnection or current disruption models of substorms. The activation of perturbed fields and plasma flows in space including the signatures of reconnection and current disruption may occur in multiple localized regions throughout the stressed tail current sheet. The activation seems to be continuously observed well after the substorm onset. These results to some extent are consistent with suggested global Alfvénic interaction considerations, in which the substorm onset is the result of Alfvénic interaction in the global current systems.

Citation: Lin, N., H. U. Frey, S. B. Mende, F. S. Mozer, R. L. Lysak, Y. Song, and V. Angelopoulos (2009), Statistical study of substorm timing sequence, *J. Geophys. Res.*, *114*, A12204, doi:10.1029/2009JA014381.

1. Introduction

[2] The onset mechanism of magnetospheric substorms is a long outstanding unsolved problem in space physics. Several substorm models, such as the near-Earth neutral line (NENL) or reconnection (Rx) model [e.g., *Hones*, 1984; *Baker et al.*, 1996; *Shiokawa et al.*, 1997], the cross-field current disruption (CD) model [*Lui*, 1996, 2004], the ballooning mode instability model [*Roux et al.*, 1991], the convection reduction model [e.g., *Lyons*, 1995], and magnetosphere-ionosphere coupling models [e.g., *Haerendel*, 1992; *Kan and Sun*, 1996], have been proposed and emphasized different aspects of substorm processes.

[3] Many efforts have been made in recent substorm studies to clarify whether substorms are triggered by magnetic reconnection (Rx) processes in the midtail region ($\sim$20–30 R_E), or by dipolarization and current disruption (CD) processes caused by the cross field current instability or other instabilities in the near-Earth region (from near the geosynchronous orbit to $\sim$10 R_E), while the subsequent development of the substorm process is then attributed to the propagation of these field and plasma disturbances out from a single onset region (compare reviews by *Lui* [2001], *Ohtani* [2004], and *Angelopoulos* [2008], and references therein). Hence much attention has been focused on the question of which physical process, CD or Rx, triggers the substorm onset, with the other process then being considered to be a consequence of the triggering process. The major scientific goal of the THEMIS mission [*Angelopoulos*, 2008; *Sibeck and Angelopoulos*, 2008] is, by accurate timing of observed signatures of Rx, CD and the auroral breakup, to determine whether substorms are triggered by CD at $\sim$10 R_E, or by Rx at $\sim$15–25 R_E. A solution to this issue would clarify the causal relationship between the two processes and the substorm onset.

[4] It is expected that in the CD model, the current disruption signatures will be first observed in the inner magnetotail, before the auroral breakup and reconnection signatures (if any) in the farther magnetotail, since the reconnection is triggered by rarefaction waves generated from the current disruption region. On the other hand in the Rx model, it is expected that reconnection signatures in the midtail regions are observed prior to the occurrences of current disruption and the auroral breakup. The time differences between observed phenomena at different locations will depend on the propagation speeds of the disturbances. It is obvious that the above timing sequences are based on the following assumptions: (1) Substorm onsets are triggered by either the CD or the Rx. (2) There is a causal relationship between CD, Rx, and substorm onset; that is, either CD causes substorm onset and Rx, or Rx causes CD and substorm onset.

[1]Space Sciences Laboratory, University of California, Berkeley, California, USA.
[2]School of Physics and Astronomy, University of Minnesota, Minneapolis, Minnesota, USA.
[3]Institute of Geophysics and Planetary Physics, University of California, Los Angeles, California, USA.

0148-0227/09/2009JA014381$09.00

[5] Each of the above models has emphasized certain aspects of the substorm process and a certain active region (near-Earth tail or in the midtail) as the initiation point. While each model has found its own observational support, they are still controversial [cf. *Lui*, 2001], and the interpretation of the observations is often inconclusive. The difficulties in the timing correlating the onset signatures of substorms in space and those on the ground have also added more controversies [e.g., *Liou et al.*, 2000, 2001; *Kepko and McPherron*, 2001; *Meng and Liou*, 2004; *Lui*, 2008]. Recent THEMIS observations have revealed that some substorm related signatures are apparently inconsistent with the single-region trigger consideration. For example, *Gabrielse et al.* [2009] reported observations of a substorm that did not start as an isolated activation in the plasma sheet or in the ionosphere. Onset took place after a series of auroral and plasma sheet activations, and the plasma sheet was active prior to substorm onset. *Nakamura et al.* [2008] reported observations of a substorm event which might imply multiple onsets corresponding to multiple activation of X lines at different X distances, not a smooth tailward retreat of an X line. An important puzzle from THEMIS observations has recently been reported: the delay time between observed space signatures (e.g., reconnection onset) and substorm onset is often too short to be accounted for by the propagation of any waves or plasma flows. For example, in the event examined by *Gabrielse et al.* [2009], the auroral breakup was observed only ~64 s after a possible substorm onset-related reconnection occurred at ~15.7 R_E; in another substorm event [*Angelopoulos*, 2008], it took ~96 s for disturbances to propagate from a reconnection site at ~20 R_E and power the auroral breakup. *Runov et al.* [2008] reported that in an event they studied the time delay between substorm onset on the ground and a substorm related tail signature at $x = -17.4$ R_E was only 20 s, which prompted the authors to suggest that an instability in the midtail plasma sheet and current disruption in the near-Earth plasma sheet may act simultaneously. With the above inconsistencies and unexplained puzzles, a different view of timing relationships needs to be explored.

2. Global Alfvénic Interaction

[6] An alternative consideration for the substorm onset has been suggested recently [*Song*, 1998, 2003; *Song and Lysak*, 2000, 2001, 2006, 2008], which emphasizes that the substorm onset is a result of Alfvénic interactions in the global current system including the tail and magnetopause current sheets as well as the auroral field-aligned current system. This global Alfvénic interaction (GAI) scenario includes the following basic physical processes and stages.

[7] 1. During the growth phase, Alfvénic interactions between the solar wind and magnetosphere throughout the magnetopause current sheet stress the magnetotail [*Song and Lysak*, 2001], leaving it susceptible to further dynamical interactions. This MHD mesoscale interaction that is associated with the rate of energy and momentum transfer from the solar wind into the magnetosphere is controlled by the solar wind–magnetosphere coupling functions which are constructed with solar wind parameters [e.g., *Perreault and Akasofu*, 1978; *Akasofu*, 1980].

[8] 2. A decrease in momentum transfer from the solar wind into the magnetosphere due to changes in the solar wind conditions produces a strong earthward body force acting in the whole magnetotail within a very short time period. As a consequence, the whole magnetotail tends to return to a more dipolar configuration releasing the previously stored free magnetic energy, and initiating fast mode waves and plasma flows. It has been noticed that substorm onsets are often triggered by changes in the orientation of the IMF [e.g., *Rostoker*, 1983; *McPherron et al.*, 1986; *Lyons*, 1995; *Hsu and McPherron*, 2002].

[9] There is a preconditioning time period from the decrease in momentum transfer to the substorm onset. This time period prepares the magnetotail for large-scale plasma reconfiguration, and the subsequent substorm auroral intensification and poleward expansion. The expansion onset is the start of the reconfiguration process. The time scale for the preconditioning stage is determined by the external driving conditions, the inertial time scale for earthward moving of the tail plasma and the Alfvén transit time for the M-I coupling. This time scale is shorter for a larger and quicker decrease in momentum transfer from the solar wind into the magnetosphere.

[10] During the preconditioning stage, the interaction between fast mode wave packets and the tail current sheet occurs in multiple regions throughout the current sheet, leading to the generation of localized shear Alfvén waves accompanied by the localized breakdown of the frozen-in condition and plasma shear flows occurring in multiple channels, as well as current sheet erosion. The produced Alfvén waves may cause auroral brightening in multiple spots in the ionosphere, giving multiple onsets before the major substorm onset. Some of these onsets in the preconditioning stage which do not develop significant poleward expansion could be classified as "pseudobreakups" [e.g., *Aikio et al.*, 1999; *Kullen and Karlsson*, 2004]. *Mende et al.* [2009] include the intensification of the preexisting equatorward arc as one of the "precursor phenomena" that occurs before the auroral poleward expansion. During and after the preconditioning stage, the newly developed force imbalance and plasma shear flows may continuously generate fast mode waves (including rarefaction waves) and Alfvén waves.

[11] 3. The expansion phase is the large-scale energy release and plasma reconfiguration in the M-I coupling system producing the substorm auroral intensification and poleward expansion. During the reconfiguration process, the interplay between the large-scale shear flows in the tail and the ionosphere will generate field-aligned currents and parallel potential drops in the auroral acceleration region causing substorm auroras.

[12] The local breakdown of the frozen-in condition, the erosion of the current sheet, and the reconfiguration of the magnetotail plasma are three distinct physical processes in space and time, although they are mutually correlated [*Song*, 1998]. These processes generate various signatures in space, like fast flows, dipolarization, heating or acceleration of particles, and waves, depending on their local magnetic topology and in situ internal and external conditions. The Alfvénic interaction may not stop after the onset of the auroral substorm. It may continue to proceed after the auroral breakup occurs; thus, onset signatures of

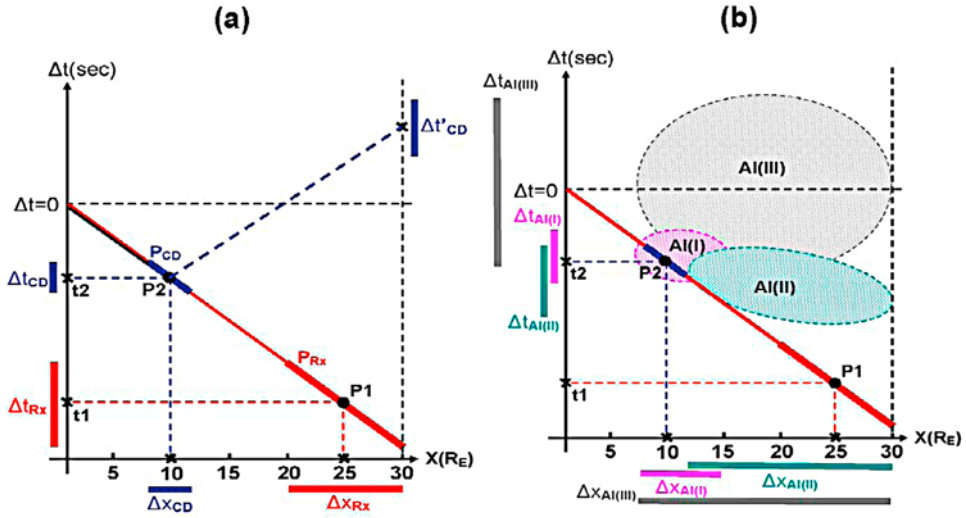

Figure 1. Schematic space-time diagram illustrating the time history of events during substorms. The ordinate represents the time delay, Δt, between the auroral substorm onset observed on the ground and the occurrence times of the associated disturbance onsets in space. The abscissa represents the locations of the observed disturbance onsets in space. The dashed line $\Delta t = 0$ corresponds to the substorm onset time. The red and blue lines indicate the travel time required for signals to propagate from a location x to the ground at a certain velocity ($\Delta x/\Delta t$), while the blue dashed line represents the travel time for tailward propagating waves. (a) Illustration of the areas where data points are expected to fall for the NENL (red) and CD (blue) models. (b) The global Alfvénic interaction mechanism of substorm onset. See text for details.

space disturbances will still be observed by spacecraft after the auroral breakup is observed on the ground.

[13] Unlike the single trigger models, this alternative GAI scenario suggests that the substorm onset results from coupled wave-related and convection-related dynamical processes covering a broad range of temporal and spatial scales in a varying driven system [*Song*, 1998]. Therefore, the substorm onset should follow a more complicated temporal sequence, requiring a new approach to analyze the timing relationship between onset signatures in different regions in the tail and auroral activity during substorms. In this paper we will perform a statistical analysis over a number of existing observations by using a space-time diagram.

3. Space-Time Diagram

[14] A scheme to examine the time sequence history of a substorm event is to plot the time delay, Δt, between the auroral substorm onset observed on the ground and the associated disturbance onsets in space versus the locations of the observed disturbance onsets in space. If a disturbance in space has caused the onset on the ground or another event in space, the time difference between these events can be no shorter than the MHD wave travel time required for the disturbance to propagate from space to the ground or between the two locations in space.

[15] Figure 1a illustrates schematically such a space-time diagram. We examine the timing of disturbance onsets in the tail from ~5 to 30 R_E, which covers substorm active regions. In this study we assume for simplicity that the disturbances propagate at a certain velocity as described later in the x direction only. The "starting time" ($\Delta t = 0$) of a substorm is defined as the most rapid development of the aurora, the start of the poleward expansion, which can be used for accurate timing. The physical significance of this starting time is that it signifies the beginning of the large-scale substorm energy dissipation in the ionosphere due to particle precipitation and auroral electrojet currents [*Mende et al.*, 2009]. Although there may exist precursor features occurring before the poleward expansion onset that are also substorm associated, they may not be suitable for accurate timing.

[16] In Figure 1a, each point represents a disturbance onset signature at a location x in space and the time difference between the space observation and the ground onset, Δt. Points that fall in the lower part of the x-Δt plane ($\Delta t < 0$) represent those space events that occur prior to the ground auroral onset, while those that fall in the region with $\Delta t > 0$ represent space signatures occurring after the ground onset. The solid lines with a constant slope connecting space locations and the ground ($x = 1$, $\Delta t = 0$) indicate the propagation of a signal at a constant speed. Time delays between signatures at two locations that have a causal relationship should be consistent with the propagation time of the disturbances traveling at an appropriate velocity.

[17] For example, a reconnection onset occurring at 25 R_E at time $t1$ prior to the ground onset is represented by point P1 on the red solid line, assuming the disturbance caused by the reconnection propagates at a constant speed represented by the reciprocal slope ($\Delta x/\Delta t$) of the red line. For space onset signatures occurring prior to the ground onset, and located between, for example, 20 and 30 R_E (marked with the red bar Δx_{Rx} in Figure 1), the time differences ($\Delta t < 0$) should fall in a time range marked by the red vertical bar Δt_{Rx} (Figure 1). It is then expected that in the reconnection

model of substorms, if the reconnection occur at ~20–30 R_E, the space signatures will produce data points in the space-time diagram clustering around the thick red line (marked with P_{Rx} in Figure 1).

[18] Similarly, for CD events occurring at ~8–12 R_E (blue bar Δx_{CD}), the time required for signals to propagate to the ground should fall in a time range Δt_{CD} (the vertical blue bar on the left). For example, a space CD onset occurring at x = 10 R_E and at time $t2$ prior to the ground onset will produce point P2 in the diagram. The CD model also suggests that tailward propagating rarefaction waves will trigger reconnection down the tail, so it would produce space signatures at farther tail locations with a certain time delay with respect to the CD occurrence time. A dashed blue line in Figure 1a correlates locations of space signatures and the onset delay times of these signatures starting at the CD onset around P2, assuming the rarefaction wave propagates at a speed equal to the reciprocal slope of the red line. Such time delays will fall in a certain range of time periods for locations at a certain x range. For example, at x = 30 R_E, the delay time range will be $\Delta t'_{CD}$, as marked by a vertical blue bar on the right. Thus, for the CD model, we expect to see in the space-time diagram data points clustering near the thick solid blue line at ~8–12 R_E (marked with P_{CD}), and data points clustering around the dashed blue line at locations farther down the tail.

[19] For the GAI mechanism, we expect different distribution pattern of data points in the space-time diagram as illustrated schematically in Figure 1b. Since the onsets of the disturbances, which are initially triggered by changes of solar wind conditions, occur at multiple locations throughout the tail current sheet, the observed locations of the disturbance onsets will cover a large part of the tail, which is marked by a gray bar (Δx_{AI}). In Figure 1b we show schematically the regions where global Alfvénic interaction processes associated with the substorm onset occur.

[20] 1. In region AI(I) (~8–12 R_E), the generation of strong field-aligned currents occurs. The substorm auroral intensification and the subsequent poleward expansion require continuously generated strong field-aligned currents, which are caused by the interplay between the ionosphere and the large-scale shear flows formed during the tail reconfiguration process. The strong field-aligned currents generated in this region may cause the substorm onset roughly on the M-I coupling time scale. The time differences ($\Delta t < 0$) should fall in a time range marked by the pink vertical bar $\Delta t_{AI(I)}$.

[21] 2. In region AI(II), the space disturbances observed at about ~15–30 R_E, represented by the green area AI(II), are mainly the signatures occurring during the preconditioning stage, which cause the later plasma sheet reconfiguration and the generation of large-scale shear flows. The corresponding space and time range ($\Delta x_{AI(II)}$ and $\Delta t_{AI(II)}$) for this region are marked by green bars.

[22] 3. In region AI(III), global Alfvénic interactions may continue to proceed for a certain time after the auroral breakup occurs. Thus we expect space signatures will also be observed in the $\Delta t > 0$ region of the space-time diagram, which is included schematically as the gray area AI(III). We also include in the AI(III) area data points with $\Delta t < 0$, for which the advanced times are too short for the signals to propagate to the ground. Space signatures associated with effects of M-I coupling and rarefaction waves also fall in this region. The range of time differences between the space signatures and the substorm onset, $\Delta t_{AI(III)}$, corresponding to the above region, is represented by the vertical gray bar on the left.

[23] The apparent time advance of the occurrence of the space signatures at ~15–30 R_E in the tail prior to the ground onset will generally be shorter than that required for disturbances to propagate from the space location to the ground. This is because the observed space signatures in the midtail region and the ground auroral onset may have no direct causal relationship. The initial substorm auroral intensification and its poleward expansion require a continuous generation of field-aligned currents and parallel potential drops. The field-aligned currents come from the interplay between the ionosphere and large-scale shear flows formed at ~8–15 R_E during the tail reconfiguration process. In the GAI scenario, the decrease of momentum transfer from the solar wind into the magnetosphere due to changes of solar wind conditions produces a strong earthward body force in the whole magnetotail within a very short time period, causing the large-scale shear flows. Thus disturbance onsets occurring at two locations (for example, at the near-Earth tail and the midtail) in general would have shorter time differences, compared to the time required for signals propagating between the two locations. On the basis of the above considerations we expect the data points resulting from the Alfvénic interaction distributed in the area AI(I) and (II) of the space-time diagram will be deflected upward from the red line.

[24] Since each substorm onset mechanism has its own expected pattern in the space-time diagram, by plotting observational data from a number of substorms on the diagram and statistically examining the distribution of space signatures associated with the substorms in the diagram, we may be able to learn how the substorm process develops.

4. Statistical Study

[25] The THEMIS mission [*Angelopoulos*, 2008] has provided a good opportunity to conduct such a study. Specially designed orbits of five identical probes allow the alignment of the satellites to detect field and plasma disturbances at a string of locations in the tail. The satellite observations are supplemented by auroral observations from a set of ground based observatories (GBO) which can be used to determine the time and the location of the auroral substorm onset [cf. *Mende et al.*, 2007, 2008]. This excellent data set is ideal for the study of the timing sequence of the substorm process.

[26] In this preliminary study, we have collected 11 substorm events and use the observed space and ground substorm onset signatures during these events to create a space-time diagram as described above. These substorm events have been carefully and comprehensively examined in detail by various authors and most of them have been reported or are in the process of publication in scientific journals. Although the data are collected by different authors, there is a common ground for the signatures collected in these studies that allows us to put them together in one space-time diagram for comparison.

[27] The first step is to determine the "onset time" of a substorm, that is the time of Δt = 0 in the diagram. This

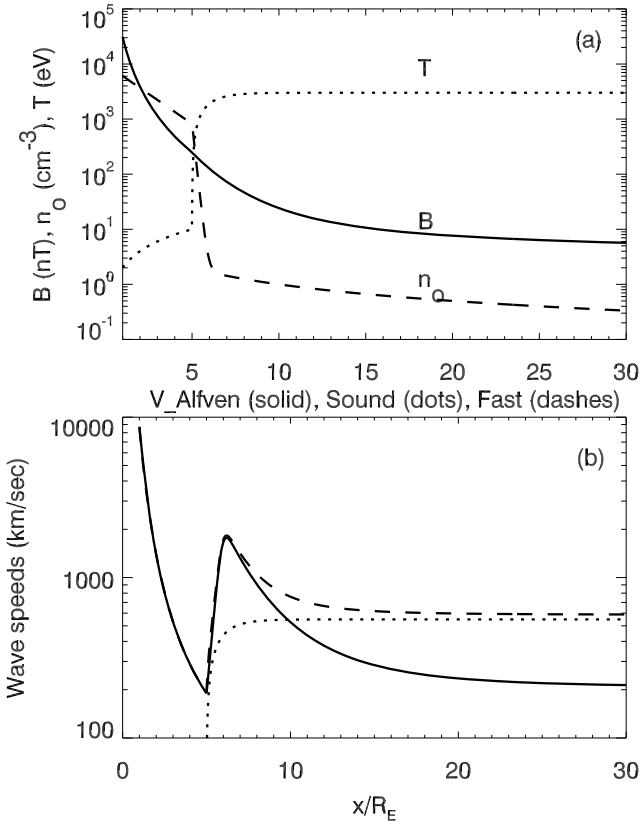

Figure 2. (a) Profiles of the magnetic field, plasma temperature, and density used in the calculation of the travel time of disturbances in space. (b) Variations of the Alfvén speed (solid line), the sound speed (dotted line), and the fast mode speed (dashed line) with the distance from the Earth, calculated with the parameters in Figure 2a.

starting point is considered to be the beginning of the large-scale substorm energy dissipation in the ionosphere. In this study we define the auroral substorm onset as the start of the auroral poleward expansion, which is likely to be timed accurately. For all of the events used in this study, the starting time was determined by examining the all-sky imager (ASI) data from THEMIS GBO and the total integrated light curve of auroral intensity, in some cases supported by the observations of the onset of Pi2 pulsations at high-latitude stations. With the auroral imaging from GBO ASI, a sudden auroral break up could be timed to the nearest imaging frame (<3 s). With the help of the total integrated light curve of auroral intensity, the auroral substorm onset time can be determined accurately within 10 s. This corresponds to a typical spatial uncertainty, for a propagation speed in the tail of ~500 km/s, of ~5000 km.

[28] The space signatures collected in this study include dipolarization, which usually is identified as an increase in B_Z and decrease in $|B_X|$, sudden intensification of magnetic field fluctuations ($T \sim 10-150$ s), and the occurrence of high-speed plasma flows. In each substorm event studied, these space signatures have been selected by their investigators for they are considered to be parts of the dynamical processes associated with the substorm, since they are related to each other or to the auroral onset on the ground. These relationships are to be examined in the space-time diagram. The connection between these disturbance onsets is thought to be accomplished by carriers of disturbance energy (plasma waves or plasma flows) that propagate between observational points at a characteristic speed. In this study we assume that the disturbances propagate across magnetic field lines in the tail plasma sheet beyond the current disruption region ($x = -10\ R_E$) at the speed of the fast mode magnetosonic wave, while within 10 R_E, they propagate along dipole magnetic field lines at the Alfvén velocity. This propagation path is similar to that described as the Tamao path [*Tamao*, 1964; *Chi et al.*, 2006].

[29] During a substorm, the magnetotail is highly disturbed, and the wave velocity may vary a lot from time to time and from one region to another. The propagation time of these waves may also be modified by the velocity of the plasma bulk flow. As an approximation, we adopt empirical equatorial profiles of the magnetic field, the plasma density and the plasma temperature to calculate the velocity and the travel time along the path. For space locations x (in R_E) < 5, the magnetic field is expressed as $B(x) = (3.11 \times 10^4\ \text{nT})/x^3$; the plasma density $n_0(x) = (10^4 m_p\ \text{cm}^{-3})e^{-x/2}$, where m_p is the proton mass; and the plasma temperature $T(x) = (2\ \text{eV}) \bullet x$. While for $x > 5$, $B(x) = (235.4\ \text{nT})/(x/5)^4 + (30\ \text{nT})/x^{1/2}$; $n_0(x) = (820 m_p\ \text{cm}^{-3})e^{-(x-5)/0.15} + (n_{ps} m_p\ \text{cm}^{-3})/x$; and $T(x) = 10\ \text{eV} + (T_{ps}\ \text{eV})(1 - e^{-(x-5)})$, where n_{ps}/x and T_{ps} are parameters approximately representing the plasma density and temperature of the plasma sheet at large x. The boundary $x = 5$ is approximately the plasmapause location. A change in this boundary location is not important in this study, since in calculating the travel time of signals from the tail, we have taken the travel path to be along dipole field lines within 10 R_E from the Earth. The variations of these equatorial parameters with the distance from the Earth are plotted in Figure 2a, where n_{ps} is taken as 10 and $T_{ps} = 3000$. These profiles are consistent with those previously published [e.g., *Chappell*, 1972; *Fairfield*, 1987; *Hughes*, 1995; *Lu et al.*, 1999; *Moore et al.*, 1987; *Slavin et al.*, 1985; *Wolf*, 1995]. Variations of the Alfvén speed, the sound speed and the fast mode speed with the distance from the Earth, calculated with the above parameters, are plotted in Figure 2b. For the propagation along the dipole field line, the density model, $n = n_0 r^{-3}$, where n_0 is the equatorial density of the field line, and r is the distance from the Earth is used, along with the true dipole field (including the angular factor) is used.

[30] In Table 1 we tabulate the occurrence times and the observation locations of the space onset signatures for the 11 events. The time differences between these signatures and the associated substorm onset times ($\Delta t = 0$) on the ground are also calculated and tabulated. For all events, the onset times are taken to be the times of the poleward expansion onset. Some authors have also used auroral intensification (AI) (a sudden increase in the auroral luminosity) [*Angelopoulos et al.*, 2008; *Gabrielse et al.*, 2009], or the onset of Pi 2 waves [*Chi et al.*, 2008] as the first indication of the start of substorms. In these cases, the AI and Pi2 onset times are given in parentheses in Table 1. These parenthetical numbers are not plotted in the space-time diagram, except for those in the "Estimated Rx Onset" column, which are plotted with concentric circles in Figure 4.

Table 1. Occurrence Times and the Observation Locations of the Space Onset Signatures for the 11 Events[a]

Aurora PWE Onset and AI	Unit of Space-Time	Inner Magnetotail				Midtail		Estimated Rx Onset
		GOES	Th A (P5)	Th E (P4)	Th D (P3)	Th C (P2)	Th B (P1)	
				26 February 2008 [Angelopoulos et al., 2008]				
0452:21 [GILL] (AI: 0451:39) (Δt: 42 s)	UT				0452:27	0450:38	0450:28	0450:03
	x (Re)				10.881	17.165	21.475	20
	Δ*t* (s)				+6 (+48)	−103 (−61)	−113 (−71)	−138 (−96)
	sign				ewf	Rx effects	Rx effects	
	UT				0453:05			
	x (Re)				10.919			
	Δ*t* (s)				+44 (+82)			
	sign				dplz			
				16 February 2008 [Gabrielse et al., 2009]				
0450:42 [SNKQ] (AI: 0450:15) (Δt: 27 s)	UT				0449:57	0449:35		∼0449:11
	x (Re)				11.015	18.283		15.6–15.9
	Δ*t* (s)				−45(−18)	−67(−40)		−91(−64)
	sign				Rx effects	Rx effects		
	UT				0450:19			
	x (Re)				11.017			
	Δ*t* (s)				−23 (+4)			
	sign				dplz			
				2 February 2008 (1) [Mende et al., 2009]				
0741:00 [GILL]	UT		0740:00	0741:09	0741:00		0743:39	0740:26
	x (Re)		8.285	11.045	11.081		29.661	14.5
	Δ*t* (s)		−60	+9	0		+159	−34
	sign		dplz;Pi	dplz;Pi	dplz;Pi		Bz < 0 twf	
				2 February 2008 (2) [Mende et al., 2009]				
0812:48 [FSIM]	UT		0813:21	0817:00	0817:00		0814:50	0811:55
	x (Re)		8.625	11.089	10.998		29.640	15.9
	Δ*t* (s)		+33	+252	+252		+122	−53
	sign		dplz;Pi ewf	dplz;Pi	dBz > 0		Bz < 0 −/+dBx	
				2 February 2008 (3) [Mende et al., 2009]				
0835:42 [FSIM]	UT		0835:24	0846:21			0837:24	0834:12
	x(Re)		8.814	11.088			29.621	14.9
	Δ*t*(s)		−18	+569			+112	−90
	sign		dplz;Pi V ∼ 200	Pi			Bz < 0 −/+dBx ewf	
				1 March 2008 (1) [Runov et al., 2008]				
0152:27 [SNKQ] (0148:45) [GBAY] (AI,Pi2) (Δt:222 s)	UT	0148:40		0148:40	0148:40	0148:25	0149:30	∼0148:05
	x (Re)	G10				17.35	22.64	15
	Δ*t* (s)					−242 (−20)	−177 (+45)	−262 (−40)
	sign					Hi E i,e flux	twf	
	UT					0148:50		
	x (Re)					17.35		
	Δ*t* (s)					−217 (5)		
	sign					twf		
				1 March 2008 (2) [Runov et al., 2008]				
0155:21 [KUUJ]	UT	0154:20		0154:20	0155:50	0155:00	0154:30	
	x (Re)	5.5 G10		8.02	9.35	17.34	22.59	
	Δ *t*(s)	−61		−61	+29	−21	−51	
	sign	dplz		dplz	dplz	twf	twf	
	UT	0153:30						
	x (Re)	4.2 G12						
	Δ*t* (s)	−111						
	sign	dplz						
				29 January 2008 (1) [Lui et al., 2008; Chi et al., 2008]				
0714:20 [FSMI]	UT			0713:15	0713:40	0712:30	0714:30	
	x (Re)			10.840	10.965	18.479	29.465	
	Δ*t* (s)			(−65)	(−40)	(−110)	(+10)	
	sign			dplz;Pi ewf150	dplz;Pi ewf700	Bz < 0	Bz < 0	
				29 January 2008 (2)				
0744:30 [FSMI] (AI: 0742:30)	UT		0745:40	0746:50	0744:40	0752:00		
	x (Re)		8.266	10.909	10.925	18.468		
	Δ*t* (s)		+70	+140	+10	+390		
	sign		dplz;Pi	dplz;Pi −/+Vx	Pi; −/+Vx	dplz;Pi		

Table 1. (continued)

Aurora PWE Onset and AI	Unit of Space-Time	Inner Magnetotail				Midtail		Estimated Rx Onset
		GOES	Th A (P5)	Th E (P4)	Th D (P3)	Th C (P2)	Th B (P1)	
				29 January 2008 (3)				
0833:15 [FSIM] (AI: 0831:30)	UT			0834:10	0834:20	0831:00		
	x (Re)			10.944	10.790	18.422		
	Δt (s)			+55	+65	−135		
	sign			dplz;Pi ewf150;Vy-200	Pi; dBx; +d|B| ewf150	Pi;dplz Ewf700		
				29 January 2008 (4)				
0838:15 [FSIM]	UT		0840:45	0834:10	0838:00	0838:10		
	x (Re)		8.789	10.944	10.775	18.416		
	Δt (s)		+150	−245	−15	−5		
	sign		+dBz;Pi Vy+200	Pi;dplz; ewf200; Vy-200	dplz;Pi twf;ewf	dplz;Pi		
	UT					0842:50		
	x (Re)					18.409		
	Δt (s)					+275		
	sign					dplz;Pi ewf200		

[a]The rows labeled "sign" list the main signatures of space disturbance at the corresponding times. dplz, dipolarization; ewf and twf, earthward flows and tailward flows, respectively; Pi, intensification of magnetic field perturbations, usually in the Pi 1–2 frequency range. "Rx effects" in the 16 and 26 February 2008 events include field and plasma variations, which are considered as reconnection signatures (see the related references for details). The time differences given in parentheses, Δt, are the time differences with respect to the AI. They are not plotted in Figure 4 except for those in the "Estimated Rx onset" column. In the 2 February 2008 events, the "Estimated Rx onset" times and locations listed are the estimation with the fast mode speed taken as 500 km/s. PWE, poleward expansion. Events occurring in the same day are numbered in parentheses in the "date" headings.

[31] There are some differences in event classification between the onset times listed in Table 1 and those in the papers cited. In the 1 March events, *Runov et al.* [2008] identified two auroral onsets (0152:27 and 0155:21) after the first sign of AI at 0148:45 UT (classified as a minor auroral onset or precursor by the authors), and correlated the space signatures before 0152:27 to the AI, while the space signatures after 0153 UT were linked to the second onset at 0155:21. Since the two auroral onsets were followed by poleward expansions, after examining the possible connection between the spacecraft locations with the locations of GBO where the auroral onsets were observed, we classified the two onsets as two substorm events and linked the space signatures to the two substorm onsets as shown in Table 1. For the events on 29 January 2008, the first activity (∼0714) was classified as "a small substorm" by *Lui et al.* [2008]. The second auroral activation identified at ∼0742 UT by *Lui et al.* [2008] is an AI as seen in FSMI auroral total intensity plots (Figure 3a) and from the global mosaic data (not shown). A poleward expansion onset was observed about two minutes later at ∼0744:30 UT. This can be seen from Figure 3a, as well as in Figures 2 and 3 of *Lui et al.* [2008]. Auroral activity continued to be strong until ∼0800 UT. About half an hour later auroral activity enhanced again and two poleward expansions were observed in all-sky imaging data from FSMI and FSIM at ∼0833:15 and 0838:15 UT (see Figure 3b), when THEMIS A, C, D, and E had their foot points close to these observatories. We have listed the above three expansion onsets as three substorm events in Table 1. Figure 3b also shows that there was strong auroral activity seen at western stations of the GBO network, FYKN and INUV, at about 0812 UT and after ∼0830 UT, which include some AIs and poleward expansions. We did not include these substorms in the statistics because the foot points of THEMIS spacecraft were relatively far from these western stations.

[32] The tabulated data are then plotted in a space-time diagram in Figure 4. Data points for the same event are plotted with the same symbols and colors. The "Estimated Rx Onset" in Table 1 is the reconnection onset time and location derived by their authors from field and plasma signatures observed at other locations. These virtual data are plotted with circles in Figure 4. The concentric circles indicate time delays between the reconnection onsets and the corresponding AIs. The dashed line at $\Delta t = 0$ marks the onset of substorms as described above. Thus the data points for signatures observed prior to the substorm onset will fall in the area of $\Delta t < 0$, while data points in $\Delta t > 0$ area are for signatures occurring after the substorm onset. The solid line represents the travel time of disturbance signals from a space location in the tail ($1 < |x| < 30\ R_E$) to the ground, calculated along the path and at velocities described above, taking $n_{ps} = 10$ and $T_{ps} = 2000$ (corresponding to a plasma density of ∼0.5 cm^{-3} and a plasma temperature of ∼2 keV at $x = -20\ R_E$). The thick dotted line which starts at $x \sim 10\ R_E$ signifies the space-time relation of signals propagating tailward, such as rarefaction waves, also assumed to be propagating at the magnetosonic velocity. In Figure 4, we only plotted the data points for those space signatures occurring within 5 min around the substorm onset; that is, $-300 \le \Delta t \le +300$ s.

[33] The travel time varies with the plasma density and temperature, and also with the magnetic field. For the 11 substorms under examination, the plasma density at ∼20 R_E is about 0.1–0.2 cm^{-3} and the temperature is varying between 300 and 3000 eV, as observed by THEMIS C. (For the events of 2 February 2008, THEMIS C plasma measurements are not available. Observations of the density and the temperature from THEMIS B at

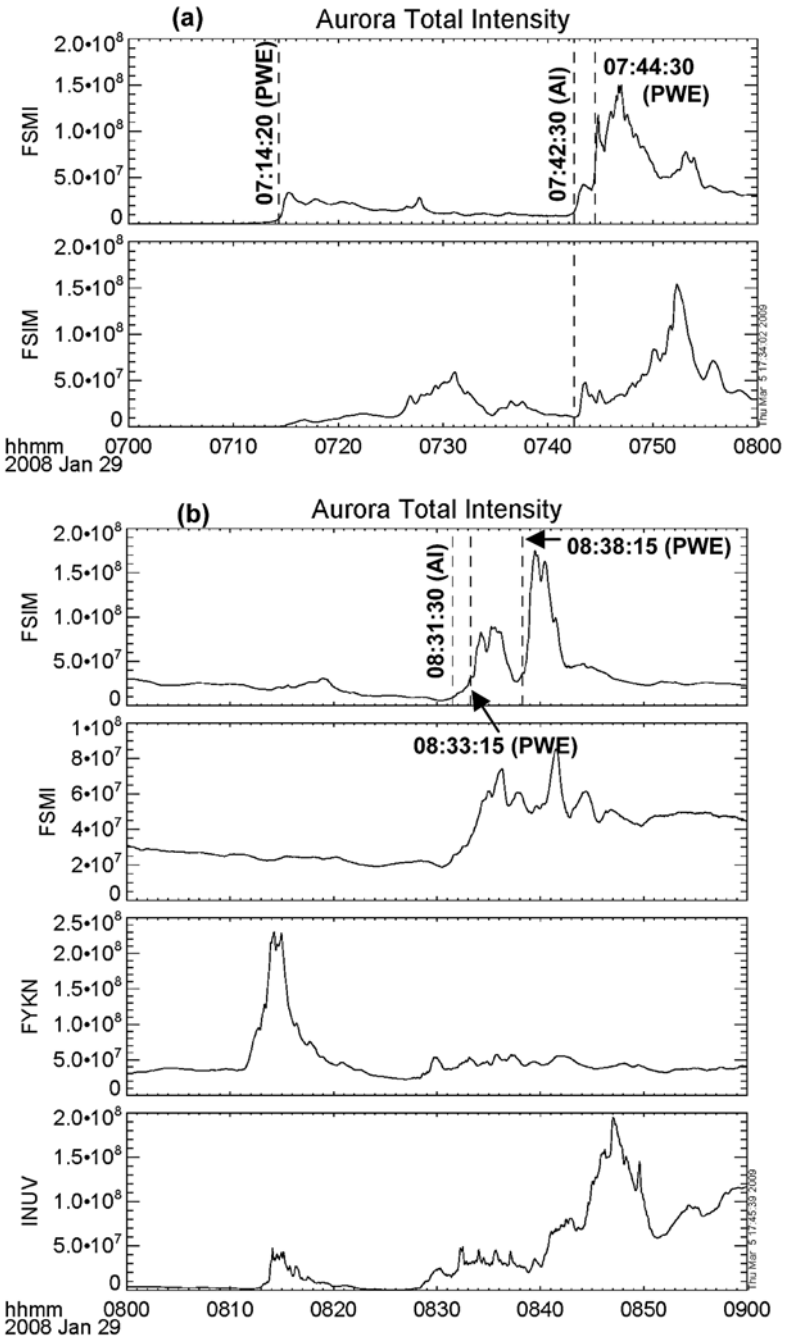

Figure 3. (a, b) Total light curves seen by the all-sky imagers at several ground observatories for the events on 29 January 2008. The vertical dashed lines indicate the occurrence times of auroral intensification (AI) and poleward expansion onset (PWE) as marked.

$\sim$30 R_E show similar variation ranges.) To cover the variation range of the travel time, we have plotted with thin dotted lines the upper and lower limits of the travel time. For the upper limit line (for the shortest travel time) we take n_{ps} = 4 and T_{ps} = 3000, which correspond to a plasma density of 0.2 cm^{-3} and a plasma temperature of $\sim$3 keV at $x = -20$ R_E. The magnetic field at $\sim$20 R_E as observed by Themis C for these events was varying with maxima of $\sim$20 nT, which are larger than the values of the model field in the central plasma sheet, and implying faster propagation velocities and shorter travel times. So in calculating the shortest limit of the travel time we have used $|\mathbf{B}|$ = 20 nT for $x > 11$ R_E. The lower limit is plotted for n_{ps} = 20 and T_{ps} = 300, which correspond to a plasma density of 1 cm^{-3} and a plasma temperature of $\sim$ 300 eV at $x = -20$ R_E. For the lower limit curve, we use the equatorial model magnetic field since the magnetic field should be the lowest in the equatorial region of the plasma

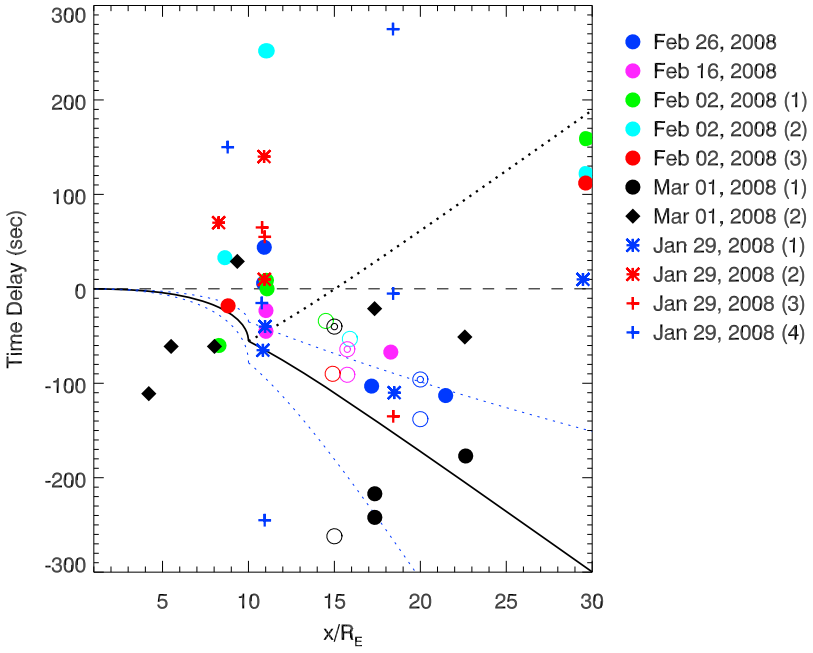

Figure 4. Data from 11 substorm events plotted in a space-time diagram. Data points for the same event are plotted with the same symbols and colors. Events occurring in the same day are numbered in parentheses as labeled in Table 1. The solid curve indicates the travel time required for signals to propagate from a tail location x to the ground at a speed calculated with the parameters in Figure 2. The two thin dotted lines mark the upper and lower limits of the travel time. The thick dotted curve represents the travel time for tailward propagating waves. See text for details.

sheet, implying the lowest propagation velocity for a certain plasma density and temperature. The calculated travel times depend critically on the parameters in the plasma sheet. We show in Figure 5 variations of the travel time with the plasma density and the temperature at 20 R_E, calculated using the profiles shown in Figure 2. For example, if the plasma sheet density at 20 R_E is $\sim$0.2 cm^{-3}, the calculated travel time for signals propagating from 30 R_E to the ionosphere could vary from 190 s to 340 s for the plasma temperature at 20 R_E ranging between 4.5 keV and 110 eV.

5. Discussion

[34] By examining each individual substorm event in Table 1, we may find evidence qualitatively supporting either the midtail initiation Rx model or near-Earth tail initiation CD model. For example, the events of 26 February (Figure 4, blue dots), 16 February (Figure 4, magenta dots), and event 1 of 29 January (Figure 4, blue stars) seem to be consistent with expected Rx model, while the time sequences for the event 1 of 1 March (Figure 4, black diamonds) and event 1 of 2 February (Figure 4, green circles) are more consistent with the CD model. But the overall scattering distribution of data points does not seem to exhibit the expected pattern for either model, especially after taking the propagation speed of signals into account. We cannot interpret the statistical data by a scenario that some substorms were generated by Rx model and others by CD model, since these two models contradict each other and should have totally different patterns in the space-time diagram. In fact, Figure 4 shows features that may not be fully explained by either model. For example, there are a number of events in the 15–25 R_E region occurring between −60 and 0 s that cannot cause auroral expansion, but likewise are too soon to be caused by a tailward propagating signal. As another example, in the 26 February event (blue circles in Figure 4), the signatures at $\sim$11 R_E (at P3; see Table 1) are after the auroral intensification; so even though the P1 and P2 signatures might look consistent with the Rx model, the question arises of why P3 is delayed. The use of the space-time diagram to do statistics on substorm timing is

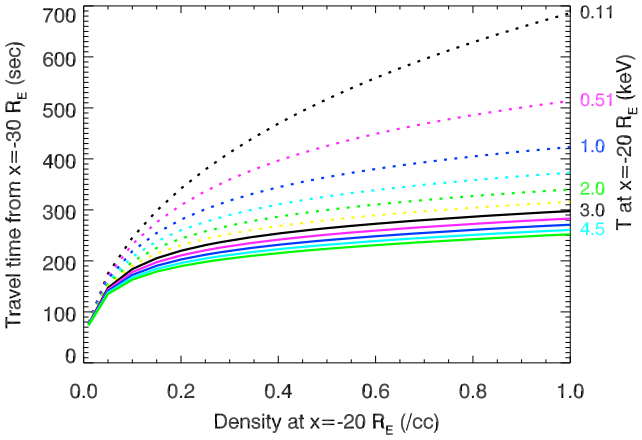

Figure 5. Variations of the travel time with the plasma density and the temperature at 20 R_E calculated using the profiles shown in Figure 2. Each curve represents the variation of the travel time with the plasma density for the plasma temperature marked on the right side with corresponding color.

to avoid analyzing individual events by selecting data according to a certain model, which may easily be subject to bias.

[35] Several features can be noticed from the space-time diagram.

[36] 1. The diagram shows that disturbance signatures near midtail ($x \sim 15-25\ R_E$) mostly occurred prior to the substorm onset. Compared to those signatures observed in near-Earth tail $x \sim 10\ R_E$, the signatures near the midtail apparently occur in the earlier stage of the substorm events. It is obvious that these midtail space signatures, which include reconnection signatures, are not triggered by disturbance onsets (e.g., dipolarization and current disruption) observed in the near-Earth tail.

[37] 2. Most of the space events that were observed prior to the substorm onset ($\Delta t < 0$) occurred in an advanced time range which was shorter than the time period needed for signals traveling from the tail locations to the ground at the calculated speed. It can be seen in the diagram that most points in $\Delta t < 0$ and $x > 15\ R_E$ area fall above the solid curve or near the upper limit line. The puzzle of the short delay time mentioned earlier seems to be a common phenomenon.

[38] There are several possibilities which may cause the apparent short delay time. The fast mode velocity in the diagram is calculated using empirical profiles of parameters in the plasma sheet. During substorms, the plasma sheet undergoes violent dynamical changes that the spacecraft sometimes may have been located in the plasma sheet boundary layer, where the fast mode velocity becomes higher. Applying an event-oriented magnetotail model [e.g., *Kubyshkina et al.*, 1999, 2002; *Lysak et al.*, 2009] may improve the accuracy of the velocity estimation. We will leave this work for future exploration. THEMIS orbits have been carefully designed so that the probes are positioned near the central plasma sheet for the tail science phase. The fast mode velocity profile we use in this study should provide an approximate estimation of the fastest speed at which signals travel in the tail. Another possibility is that the disturbance signals were riding plasma flows such as bursty bulk flows that accelerate the propagation of the signals. But the plasma flows are likely to attenuate in the path and most fast plasma flows may not reach geosynchronous orbit [*Ohtani et al.*, 2006]. A carrier that may propagate faster than the fast mode waves is the kinetic Alfvén wave. Kinetic Alfvén waves have a faster group velocity than MHD Alfvén waves but also suffer wave damping [*Lysak and Song*, 2003; *Lysak and Lotko*, 1996].

[39] A viable explanation of the short delay time is that the observed disturbance onsets in the tail may not directly link to the substorm auroral onsets observed on the ground. The above possibility is a natural consequence of the GAI mechanism of substorm onset. As described in the GAI scenario above, a decrease of the momentum transfer from the solar wind into the magnetosphere due to changes in solar wind conditions produces a strong earthward body force acting on the whole magnetotail from the near-Earth to midtail regions within a very short time period, causing localized disturbances of the fields and flows, as well as the large-scale shear flows. As a consequence, the whole magnetotail tends to return to a more dipolar configuration releasing the previously stored free magnetic energy, and initiating fast mode waves and plasma shear flows. Thus two events in space that are triggered externally may not be related (to have a simple causal relationship) to each other. The separation between the occurrence times of disturbance onsets at two locations (especially for two widely separated locations, like the near-Earth tail and the midtail) may thus be shorter than the time needed for signals to travel between the two locations. We have defined the onset time of a substorm (the time of $\Delta t = 0$ in the diagram) as the start of the auroral poleward expansion. As mentioned previously, some authors have also used auroral intensification (AI) as the first indication of the start of substorms. If we chose the start of AI as the time of $\Delta t = 0$, it would generally move all points upward in the diagram, which would make the delay time between the ground auroral onsets and the tail disturbance onsets even shorter. In that case the agreement with the simple propagation model would be even worse.

[40] In general, the initial arc brightening in the most equatorward edge during the substorm onset is directly associated with the generation of the field-aligned current in the near-Earth tail ($\sim 8-12\ R_E$), but the shear flows associated with the field-aligned currents are driven by the body force in the near-Earth tail or the integrated body force of the whole tail. The poleward expansion of the auroral arcs after the substorm onset is related to the reconfiguration processes of the whole tail. It is noticed that both CD and Rx models emphasize the internal triggers due to instabilities or other localized processes. The GAI scenario emphasizes not only the internal Alfvénic interaction processes, such as the M-I coupling process, but also the external trigger process. Thus in the GAI scenario, the magnetotail is a driven system. Also, we notice that the substorm onset is characterized by the explosive release of the energy stored in the tail during the growth phase and the plasma sheet reconfiguration. It seems unlikely that a localized reconnection at the midtail or a CD onset in the near Earth can cause the large-scale plasma sheet reconfiguration without a decrease of the momentum transfer from the solar wind into the magnetosphere.

[41] 3. Some space signatures occurred well after the substorm onset ($\Delta t > 0$). Most of these space signatures were detected by THEMIS D and E, which were positioned at $8 < x < 12\ R_E$ in the tail. In the diagram, there are a few events detected at $x \sim 30\ R_E$. These signatures were interpreted by their observers as the possible effects of reconnection occurring earthward of the spacecraft. Space signatures observed near or after the substorm onset may also result from the effects of rarefaction waves. Many of these signatures are dipolarization signatures. The fact that these signatures are often observed in the near-Earth tail ($x \sim 10\ R_E$) may imply that the rarefaction waves do not reach the midtail region easily; otherwise we would see more points near and above the dotted line in the midtail region. Another possibility of producing space signatures near or after the substorm onset (data points falling near or above the $\Delta t = 0$ line) is the continuous operation of Alfvénic interaction between fast mode waves and the tail current sheet under varying external and internal conditions, which does not stop after the time of substorm onset.

[42] This statistical study is preliminary, collecting only 11 substorms. Most of these events have been carefully examined by different authors. Although there are some

incongruities in identifying and classifying events among the authors, we still found physical common ground which allowed us to compare these events and examine them in the space-time diagram. The inaccuracy in the distribution pattern of data points in the diagram would be reduced by increasing the number of events and adopting more consistent identification and classification of events, which is a task of ongoing work. The distribution pattern of events is also affected by the limited number of observations for the same event. Mapping of the foot points of magnetic field lines threading the spacecraft may also produce errors in correlating space and ground signatures. While the THEMIS mission has provided excellent observations based on the conjunction of five points in space and ground auroral activity, we may still need more multipoint observations in both radial and longitudinal range. These difficulties have to be resolved in future studies, maybe by appealing to further quantitative theoretical calculations and possible high-resolution simulations.

6. Concluding Remarks

[43] We have introduced and demonstrated a novel statistical approach to study the timing sequence of substorm processes by using a space-time diagram, where onsets of space signatures associated with substorms are correlated with the auroral substorm onset on the ground. The observed delay times between space and ground signatures are plotted versus the locations of space observations in the diagram, and the distribution pattern of data points is compared with expected patterns predicted by various substorm onset mechanisms.

[44] The diagram shows that, while most of the space signatures in the midtail region are detected in the earlier stage of the substorms than those in the near-Earth tail region, the observed delay times between space and ground signatures seem to be shorter than the time expected. We have suggested that the apparent short delay time arises because the observed space signatures in the midtail region and the ground auroral onset may not have a simple causal relationship. Instead, it is the decrease in momentum transfer from the solar wind into the magnetosphere due to changes of the solar wind conditions that is directly related to the generation of field-aligned current in the near-Earth tail region causing the substorm onset. This interpretation is consistent with the physical picture depicted by the GAI scenario. The distribution of data points prior to the substorm onset in the space-time diagram can be roughly represented by regions AI(I) and (II) in Figure 1b. The space signatures occurring at $\Delta t < 0$ but near the $\Delta t = 0$ line are evidence that the observed space disturbances may not directly link to the onset of substorm. They are likely to be the disturbance onsets in the tail that occur near the auroral substorm onset time and are triggered by the force generated by changes of the solar wind conditions. Together with the signatures observed after the substorm onset ($\Delta t > 0$), they can be schematically represented by region AI(III) in Figure 1b that covers continuous occurrences of Alfvénic interactions under varying external and internal conditions around the substorm onset.

[45] The results of this preliminary study show that unlike that suggested in Rx or CD models, where substorm onset is triggered by either Rx or CD and followed by a simple causal chain of events, the observed substorm onset signatures seem to follow a more complicated temporal sequence, which may be controlled by global Alfvénic interactions in the solar wind–magnetosphere-ionosphere coupled system, where the substorm onset results from wave-related and convection-related dynamical processes covering a broad range of temporal and spatial scales in a varying driven system. Our statistical analysis approach using the space-time diagram is an attempt to understand these different dynamical processes associated with the substorm onset.

[46] **Acknowledgments.** The work done at the University of California at Berkeley was supported by NASA grants NAS5–02099, NNG05GL27G-01/09, and NNX09AJ75G. The work done at the University of Minnesota was supported by NASA grant NNX08AM31G. The authors are very grateful to C. Gabrielse, R. Nakamura, P. Chi, and A. Runov for providing their PowerPoint presentations on the events they studied before their papers are published. The authors thank the referees for their thoughtful and constructive comments and suggestions. N.L. would like to thank P. Chi, A. Runov, and G. Parks for helpful discussions.

[47] Wolfgang Baumjohann thanks Kazue Takahashi and Peter Chi for their assistance in evaluating this paper.

References

Aikio, A. T., V. A. Sergeev, M. A. Shukhtina, L. I. Vagina, V. Angelopoulos, and G. D. Reeves (1999), Characteristics of pseudobreakups and substorms observed in the ionosphere, at the geosynchronous orbit, and in the midtail, *J. Geophys. Res.*, *104*(A6), 12,263–12,287, doi:10.1029/1999JA900118.

Akasofu, S.-I. (1980), The solar wind–magnetosphere energy coupling and magnetosphere disturbances, *Planet. Space Sci.*, *28*, 495–509, doi:10.1016/0032-0633(80)90031-8.

Angelopoulos, V. (2008), The THEMIS Mission, *Space Sci. Rev.*, *141*, 5–34, doi:10.1007/s11214-008-9336-1.

Angelopoulos, V., et al. (2008), Tail reconnection triggering substorm onset, *Science*, *321*, 931–935, doi:10.1126/science.1160495.

Baker, D. N., T. I. Pulkkinen, V. Angelopoulos, W. Baumjohann, and R. L. McPherron (1996), Neutral line model of substorms: Past results and present view, *J. Geophys. Res.*, *101*(A6), 12,975–13,010, doi:10.1029/95JA03753.

Chappell, C. R. (1972), Recent satellite measurements of the morphology and dynamics of the plasmasphere, *Rev. Geophys.*, *10*, 951–979, doi:10.1029/RG010i004p00951.

Chi, P. J., D.-H. Lee, and C. T. Russell (2006), Tamao travel time of sudden impulses and its relationship to ionospheric convection vortices, *J. Geophys. Res.*, *111*, A08205, doi:10.1029/2005JA011578.

Chi, P. J., S. Ohtani, C. T. Russell, V. Angelopoulos, and K.-H. Glassmeier (2008), A magnetoseismic investigation of substorm onsets and its validation by satellite observations, *Eos Trans. AGU*, *89*(53), Fall Meet. Suppl., Abstract SM43A–1716.

Fairfield, D. H. (1987), Structure of the geomagnetic tail, in *Magnetotail Physics*, edited by A. T. Y. Lui, pp. 23–33, Johns Hopkins Univ. Press, Baltimore, Md.

Gabrielse, C., et al. (2009), Timing and localization of near-Earth tail and ionospheric signatures during a substorm onset, *J. Geophys. Res.*, *114*, A00C13, doi:10.1029/2008JA013583.

Haerendel, G. (1992), Disruption, ballooning or auroral avalanche: On the cause of substorms, in *Proceedings of the First International Conference on Substorms (ICS-1)*, *Eur. Space Agency Spec. Publ.*, *ESA SP-335*, 417–420.

Hones, E. W., Jr. (1984), Plasma sheet behaviour during substorms, in *Magnetic Reconnection in Space and Laboratory Plasmas*, *Geophys. Monogr. Ser.*, vol. 30, edited by E. W. Hones Jr., pp. 178–184, AGU, Washington, D. C.

Hsu, T.-S., and R. L. McPherron (2002), An evaluation of the statistical significance of the association between northward turnings of the interplanetary magnetic field and substorm expansion onsets, *J. Geophys. Res.*, *107*(A11), 1398, doi:10.1029/2000JA000125.

Hughes, W. J. (1995), The magnetopause, magnetotail and magnetic reconnection, in *Introduction to Space Physics*, edited by M. G. Kivelson and C. T. Russell, pp. 227–287, Cambridge Univ. Press, New York.

Kan, J. R., and W. Sun (1996), Substorm expansion phase caused by an intense localized convection imposed on the ionosphere, *J. Geophys. Res.*, *101*(A12), 27,271–27,281, doi:10.1029/96JA02426.

Kepko, L., and R. L. McPherron (2001), Comment on "Evaluation of low-latitude Pi2 pulsations as indicators of substorm onset using Polar ultraviolet imagery" by K. Liou et al., *J. Geophys. Res.*, *106*(A9), 18,919–18,922, doi:10.1029/2000JA000189.

Kubyshkina, M. V., V. A. Sergeev, and T. I. Pulkkinen (1999), Hybrid Input Algorithm: An event-oriented magnetospheric model, *J. Geophys. Res.*, *104*(A11), 24,977–24,993, doi:10.1029/1999JA900222.

Kubyshkina, M. V., V. A. Sergeev, S. V. Dubyagin, S. Wing, P. T. Newell, W. Baumjohann, and A. T. Y. Lui (2002), Constructing the magnetospheric model including pressure measurements, *J. Geophys. Res.*, *107*(A6), 1070, doi:10.1029/2001JA900167.

Kullen, A., and T. Karlsson (2004), On the relation between solar wind, pseudobreakups, and substorms, *J. Geophys. Res.*, *109*, A12218, doi:10.1029/2004JA010488.

Liou, K., C.-I. Meng, P. T. Newell, K. Takahashi, S.-I. Ohtani, A. T. Y. Lui, M. Brittnacher, and G. Parks (2000), Evaluation of low-latitude Pi2 pulsations as indicators of substorm onset using Polar ultraviolet imagery, *J. Geophys. Res.*, *105*(A2), 2495–2505, doi:10.1029/1999JA900416.

Liou, K., P. T. Newell, C.-I. Meng, K. Takahashi, S.-I. Ohtani, A. T. Y. Lui, M. Brittnacher, and G. Parks (2001), Reply to comment by L. Kepko and R. L. McPherron on "Evaluation of low-latitude Pi2 pulsations as indicators of substorm onset using Polar ultraviolet imagery", *J. Geophys. Res.*, *106*(A9), 18,923–18,926, doi:10.1029/2000JA000362.

Lu, G., N. A. Tsyganenko, A. T. Y. Lui, H. J. Singer, T. Nagai, and S. Kokubun (1999), Modeling of time-evolving magnetic fields during substorms, *J. Geophys. Res.*, *104*(A6), 12,327–12,337, doi:10.1029/1999JA900145.

Lui, A. T. Y. (1996), Current disruption in the Earth's magnetosphere: Observations and models, *J. Geophys. Res.*, *101*(A6), 13,067–13,088, doi:10.1029/96JA00079.

Lui, A. T. Y. (2001), Current controversies in magnetospheric physics, *Rev. Geophys.*, *39*, 535–563, doi:10.1029/2000RG000090.

Lui, A. T. Y. (2004), Potential plasma instabilities for substorm expansion onsets, *Space Sci. Rev.*, *113*, 127–206, doi:10.1023/B:SPAC.0000042942.00362.4e.

Lui, A. T. (2008), Re-evaluation of observations for the February 26, 2008 substorm reported to show tail reconnection triggering substorm expansion onset, *Eos Trans. AGU*, *89*(53), Fall Meet. Suppl., Abstract SM43A–1722.

Lui, A. T. Y., et al. (2008), Determination of the substorm initiation region from a major conjunction interval of THEMIS satellites, *J. Geophys. Res.*, *113*, A00C04, doi:10.1029/2008JA013424.

Lyons, L. R. (1995), A new theory for magnetospheric substorms, *J. Geophys. Res.*, *100*(A10), 19,069–19,081, doi:10.1029/95JA01344.

Lysak, R. L., and W. Lotko (1996), On the kinetic dispersion relation for shear Alfvén waves, *J. Geophys. Res.*, *101*(A3), 5085–5094, doi:10.1029/95JA03712.

Lysak, R. L., and Y. Song (2003), Kinetic theory of the Alfvén wave acceleration of auroral electrons, *J. Geophys. Res.*, *108*(A4), 8005, doi:10.1029/2002JA009406.

Lysak, R. L., Y. Song, and T. W. Jones (2009), Propagation of Alfvén waves in the magnetotail during substorms, *Ann. Geophys.*, *27*, 2237–2246.

McPherron, R. L., T. Terasawa, and A. Nishida (1986), Solar wind triggering of substorm expansion onset, *J. Geomagn. Geoelectr.*, *38*(11), 1089–1108.

Mende, S. B., V. Angelopoulos, H. U. Frey, S. Harris, E. Donovan, B. Jackel, M. Syrjaesuo, C. T. Russell, and I. Mann (2007), Determination of sub-storm onset timing and location using the THEMIS ground based observatories, *Geophys. Res. Lett.*, *34*, L17108, doi:10.1029/2007GL030850.

Mende, S. B., et al. (2008), The THEMIS array of ground-based observatories for the study of auroral substorms, *Space Sci. Rev.*, *141*, 357–387, doi:10.1007/s11214-008-9380.

Mende, S. B., V. Angelopoulos, H. U. Frey, E. Donovan, B. Jackel, K.-H. Glassmeier, J. P. McFadden, D. Larson, and C. W. Carlson (2009), Timing and location of substorm onsets from THEMIS satellite and ground based observations, *Ann. Geophys.*, *27*, 2813–2830.

Meng, C.-I., and K. Liou (2004), Substorm timings and timescales: A new aspect, *Space Sci. Rev.*, *113*, 41–75, doi:10.1023/B:SPAC.0000042939.88548.68.

Moore, T. E., D. L. Gallagher, J. L. Horwitz, and R. H. Comfort (1987), MHD wave breaking in the outer plasmasphere, *Geophys. Res. Lett.*, *14*, 1007–1010, doi:10.1029/GL014i010p01007.

Nakamura, R., et al. (2008), Fast flow signatures during multiple activation of Feb. 16, 0220 UT substorm, paper presented at The First Joint Cluster–THEMIS Science Workshop, Univ. of N. H., Durham, N. H.

Ohtani, S. (2004), Flowbursts in the plasma sheet and auroral substorm onset: Observational constraints on connection between midtail and near-Earth substorm processes, *Space Sci. Rev.*, *113*, 77–96, doi:10.1023/B:SPAC.0000042940.59358.2f.

Ohtani, S., H. J. Singer, and T. Mukai (2006), Effects of the fast plasma sheet flow on the geosynchronous magnetic configuration: Geotail and GOES coordinated study, *J. Geophys. Res.*, *111*, A01204, doi:10.1029/2005JA011383.

Perreault, P., and S.-I. Akasofu (1978), Study of geomagnetic storms, *Geophys. J. R. Astron. Soc.*, *54*, 547–573.

Rostoker, G. (1983), Triggering of expansive phase intensifications of magnetospheric substorms by northward turnings of the interplanetary magnetic field, *J. Geophys. Res.*, *88*(A9), 6981–6993, doi:10.1029/JA088iA09p06981.

Roux, A., S. Perraut, P. Robert, A. Morane, A. Pedersen, A. Korth, G. Kremser, B. Aparicio, D. Rodgers, and R. Pellinen (1991), Plasma sheet instability related to the westward traveling surge, *J. Geophys. Res.*, *96*(A10), 17,697–17,714, doi:10.1029/91JA01106.

Runov, A., et al. (2008), Multipoint in situ and ground-based observations during auroral intensifications, *J. Geophys. Res.*, *113*, A00C07, doi:10.1029/2008JA013493.

Shiokawa, K., W. Baumjohann, and G. Haerendel (1997), Braking of high-speed flows in the near-Earth tail, *Geophys. Res. Lett.*, *24*, 1179–1182, doi:10.1029/97GL01062.

Sibeck, D. G., and V. Angelopoulos (2008), THEMIS science objectives and mission phases, *Space Sci. Rev.*, *141*, 35–59, doi:10.1007/s11214-008-9393-5.

Slavin, J. A., E. J. Smith, D. G. Sibeck, D. N. Baker, R. D. Zwickl, and S.-I. Akasofu (1985), An ISEE-3 study of average and substorm conditions in the distant magnetotail, *J. Geophys. Res.*, *90*(A11), 10,875–10,895, doi:10.1029/JA090iA11p10875.

Song, Y. (1998), Theoretical constraints on mechanisms for the substorm current wedge, in *Substorms 4*, edited by S. Kokubun and Y. Kamide, pp. 543–546, Terra Sci., Tokyo.

Song, Y. (2003), Challenge to the magnetic reconnection hypothesis, in *Proceedings of the Magnetic Reconnection Meeting*, *IRF Sci. Rep. 280*, edited by R. Lundin and R. McGregor, pp. 25–35, Swed. Inst. of Space Phys., Kiruna, Sweden.

Song, Y., and R. L. Lysak (2000), Paradigm transition in cosmic plasma physics, magnetic reconnection and the generation of field-aligned current, in *Magnetospheric Current Systems*, *Geophys. Monogr. Ser.*, vol. 118, edited by S.-I. Ohtani et al., pp. 11–19, AGU, Washington, D. C.

Song, Y., and R. L. Lysak (2001), Towards a new paradigm: From a quasi-steady description to a dynamical description of the magnetosphere, *Space Sci. Rev.*, *95*, 273–292, doi:10.1023/A:1005288420253.

Song, Y., and R. L. Lysak (2006), Displacement current and the generation of parallel electric fields, *Phys. Rev. Lett.*, *96*, 145002, doi:10.1103/PhysRevLett.96.145002.

Song, Y., and R. L. Lysak (2008), Global Alfvénic interaction and substorm onset, *Eos Trans. AGU*, *89*(53), Fall Meet. Suppl., Abstract SM43A–1715.

Tamao, T. (1964), The structure of three-dimensional hydromagnetic waves in a uniform cold plasma, *J. Geomagn. Geoelectr.*, *16*, 89–114.

Wolf, R. A. (1995), Magnetospheric configuration, in *Introduction to Space Physics*, edited by M. G. Kivelson and C. T. Russell, pp. 288–329, Cambridge Univ. Press, New York.

V. Angelopoulos, Institute of Geophysics and Planetary Physics, University of California, Los Angeles, CA 90095, USA.

H. U. Frey, N. Lin, S. B. Mende, and F. S. Mozer, Space Sciences Laboratory, University of California, 7 Gauss Way, Berkeley, CA 94720-7450, USA. (nlin@ssl.berkeley.edu)

R. L. Lysak and Y. Song, School of Physics and Astronomy, University of Minnesota, Minneapolis, MN 55455, USA.